Biosensors and Bioelectronics 146 (2019) 111751

Contents lists available at ScienceDirect

Biosensors and Bioelectronics

journal homepage: http://www.elsevier.com/locate/bios

Highly sensitive nitrite sensor based on AuNPs/RGO nanocomposites modified graphene electrochemical transistors

Yang Zhou [a,1], Mingyu Ma [a,1], Hanping He [b], Zhiwei Cai [a], Nan Gao [a], Chaohui He [a], Gang Chang [a,*], Xianbao Wang [a], Yunbin He [a,**]

[a] Ministry-of-Education Key Laboratory for the Green Preparation and Application of Functional Materials, Hubei Key Laboratory of Polymer Materials, School of Materials Science and Engineering, Hubei University, No.368 Youyi Avenue, Wuchang, Wuhan, 430062, China
[b] Ministry of Education Key Laboratory for the Synthesis and Application of Organic Functional Molecules, College of Chemistry and Chemical Engineering, Hubei University, No. 368 Youyi Avenue, Wuchang, Wuhan, 430062, China

ARTICLE INFO

Keywords:
Electrochemical transistors
Au nanoparticles
Graphene
Nitrite
Nonenzymic sensors

ABSTRACT

Detection of nitrite is important for environmental safety and human health, and the development of high-performance sensors for accurate detection of nitrite is highly desirable. Herein, a highly sensitive graphene electrochemical transistor (GECT) nitrite sensor was designed and fabricated for the first time. A single layer of graphene was placed between the source and drain electrodes by the wetting transfer method to act as channel for the transistor. Au nanoparticles modified reduced graphene oxide nanocomposites (AuNPs/RGO) were electrodeposited at the transistor gate to improve its catalytic oxidation performance of nitrite with optimized electrodeposition conditions. The sensing principle was attributed to changes in effective gate voltage applied to GECT induced by electrooxidation of nitrite at gate electrodes. Due to the high carrier mobility of graphene in the channel and the excellent electrocatalytical activity of AuNPs/RGO on the gate, the obtained sensor device exhibited an exceedingly low detection limit (0.1 nM nitrite) and ultra-wide linear range from 0.1 nM to 7 μM and from 7 to 1000 μM, which are comparable or superior to the performance of large-scale instruments (e.g. chromatography, spectrophotometry, and spectrofluorimetry etc.). The GECT device also showed good anti-interference performance toward common interfering ions and stable performances. Nitrite in natural lake water has been proven to be monitored by our devices. Therefore, the present novel GECT sensor could act as a desirable practical platform for highly sensitive detection of nitrite in the food and environmental fields.

1. Introduction

Nitrite is an important source of nitrogen in green plants and intermediate by-products in nitrogen cycle. It is also widely present in environment, soil and water, and employed in various foods as preservative (Radhakrishnan et al., 2014; Wolfe and Patz, 2002). Nitrite at moderate concentration does not cause concerns but high levels of Nitrite in the human body could interact with haemoglobin to form methaemoglobin, a molecule that inhibits haemoglobin from transporting oxygen throughout the body and cause tissue hypoxia. Nitrite can also react with secondary amine, tertiary amine and amide to form nitrosamines, known for their carcinogenic properties. Therefore, the determination of nitrite levels is important in both environmental monitoring and food analysis.

Several methods have been utilized for nitrite determination, including spectrophotometry (Bru et al., 2006), chromatography (Kodamatani et al., 2009), Raman spectroscopy (Mahajan et al., 2007), chemiluminescence (Mikuška and Večeřa, 2003), and spectrofluorimetry (Büldt and Karst, 1999). However, these techniques suffer from several limitations for practical applications in terms of complexity of pretreatment procedures and time-consumption of extraction processes (Afkhami et al., 2014). By comparison, electrochemical methods might provide simpler, faster, and sensitive real-time detection. However, the detection limits of conventional electrochemical methods are not low enough for detection of nitrite. They could not meet the demanding requirements of sensitivity and detection limits in quality

* Corresponding author.
** Corresponding author.
E-mail addresses: gchanghubei@gmail.com (G. Chang), ybhe@hubu.edu.cn (Y. He).
[1] These authors contributed equally to this work.

https://doi.org/10.1016/j.bios.2019.111751
Received 22 July 2019; Received in revised form 29 September 2019; Accepted 30 September 2019
Available online 1 October 2019

monitoring of water such as drinking mineral water. Therefore, the development of rapid and reliable methods for nitrite detection is of high importance.

Electrochemical transistor sensors are relatively new electrochemical detection devices with promising sensitivities due to their inherent amplification characteristics (Berggren and Richter-Dahlfors, 2007; Yan et al., 2014; Quhe et al., 2019). In particular, organic electrochemical transistors (OECT) can be used in aqueous solutions at low operating voltages to yield very stable performances (Faria et al., 2017; Liao and Yan, 2013; Lin and Yan, 2012). Therefore, OECTs have broadly been considered for highly sensitive and low cost biosensors, including biosensors for detection of glucose (Liao et al., 2013; Liao et al., 2015a), dopamine (Tang et al., 2011; Zhang et al., 2014), uric acid (Liao et al., 2015b), ions (Lin et al., 2010), ascorbic acid (Zhang et al., 2018b), bacteria (He et al., 2012), cells (Hempel et al., 2017), and various proteins (Estrela et al., 2010). Electrochemical transistors would likely be highly sensitive devices for nitrite detection. However, this electrochemical transistor has not been so far considered for nitrite determination.

In this study, graphene electrochemical transistors (GECTs) with Au nanoparticles/reduced graphene oxide (AuNPs/RGO) nanocomposites-modified glassy carbon as gate electrode were prepared and applied for the detection of nitrite. GECTs are often classified as a category of OECTs because of their consistency with OECTs in structure. The monolayer graphene film was used as channel due to its narrow bandgap and high mobility. The catalytic materials at the gate electrode combined excellent electrocatalytic properties of AuNPs with high specific surface area of RGO. This induced synergistic effect in AuNPs/RGO nanocomposites, leading to enhanced electrocatalytic capabilities (Shu et al., 2015). The novel AuNPs/RGO modified gate electrode was introduced into the graphene electrochemical transistor (GECT) device and it was the first time that the GECT was designed and fabricated a sensor for nitrite detection. Different deposition methods were compared to optimize the experiment conditions. The electrocatalysts on gate electrode prepared by different experimental processing were fully demonstrated to have a great influence on the sensing performance of the device. Repeating tests were also carried out to determine reproducibility and stability of the GECT sensor. The nitrite samples with different concentrations prepared by the water of East Lake (Wuhan, China) were innovative tested. The results suggested that the novel AuNPs/RGO-modified glassy carbon gated GECT could offer a fast and simple platform for nitrite detection with high sensitivity, fast response, and wide detection range.

2. Experimental

2.1. Materials

Monolayer graphene was purchased from Hefei Vigon Material Technology, $HAuCl_4 \cdot 3H_2O$ from Aldrich, Au from Zhongnuo Advanced Material Technology, Graphene oxide from XFNANO, PMMA from Shanghai Macklin Biochemical, Nafion (5%) from Du Pont, and Chitosan from Aladdin Industrial. $NaNO_2$, $Fe(NO_3)_3 \cdot 9H_2O$, $Na_2HPO_4 \cdot 12H_2O$, $NaH_2PO_4 \cdot 2H_2O$, NaCl, KCl, NH_4Cl, $CaCl_2$, $MgCl_2$, Na_2SO_4, Na_3PO_4, CH_3COOH, CH_3COONa, glucose and acetone were all obtained from Sinopharm Chemical Reagent. All chemicals were of analytical grade. Phosphate buffer solution (PBS, 0.1 M, pH = 7.4) was prepared from Na_2HPO_4 and NaH_2PO_4. The nitrite and interfering substances solutions were obtained using PBS solution immediately before experiments. Pure water obtained with Kertone Ultrapure Water System P60-CY (Kertone Water Treatment) was used in all experiments.

2.2. Device fabrication

The structural schematic diagram of GECT nitrite sensor can be seen from Fig. 1A. Glass was used as substrate of the device. And Au was deposited by thermal evaporation using mask as drain and source electrodes, as shown in Fig. 1B. The length and width of the channel (between the drain and source electrodes) were set at 6 mm and 0.25 mm, respectively. Wet transfer approach was employed to assemble the graphene monolayer on top of the source and drain electrodes as channel of the device (Hao et al., 2017; Wang et al., 2018a,b,c). The wet transfer process is schematically shown in Fig. S1. Typically, polymethyl methacrylate (PMMA, 70 mg/mL) anisole solution was first dropped onto the single-layer graphene supported on copper substrate, and then spin-coated onto the graphene by homogenization to protect integrity of the graphene monolayer. The graphene was cut into pieces with 3×3 mm in size, and then transferred back to surface of 0.7 M ferrite nitrate solution for etching off the copper substrate in 3 h. After washing three times with ultra-pure water, a single layer of graphene protected by PMMA thin film was obtained. Before transferring the monolayer graphene, the glass slide substrate was treated with oxygen plasma for 180s to improve film adhesion (Tang et al., 2011; Lin et al., 2017, 2019; Wei et al., 2018). Thereafter, the single layer of graphene with PMMA film was transferred on top of the source and drain electrodes of the transistor. After drying of graphene in air at room temperature, the device was annealed for half an hour at 90 °C, and then soaked in acetone at 60 °C for 3h to dissolve the protecting PMMA film on top of the single-layer graphene and yield the main part of GECT.

Next, the assembled GECT was clamped on the bottom of a specially designed container with funnel shape and diameter of 3 mm (Fig. 1B). The glassy carbon electrode (GCE) was then inserted from top of the container containing PBS for electrochemical testing as gate electrode of the GECT. To combine the excellent electrocatalytic properties AuNPs and high specific surface area of RGO, AuNPs/RGO nanocomposites were deposited on GCE surface to form the gate electrode through one-step electrodeposition. This procedure started from the preparation of aqueous electro-deposition solution by 10 mM $HAuCl_4$, 0.5 mg/mL graphene oxide, and 0.1 M KCl. The GCE was then immersed into the solution, and AuNPs/RGO nanocomposites were deposited on the surface of GCE under different electrodeposition conditions. Finally, the AuNPs/RGO-modified GCE was thoroughly cleaned by deionized water and dried at ambient conditions for future use.

2.3. Characterization

The electrodeposition process was carried out on an electrochemical workstation (CHI660e, CH Instruments). Semiconductor parameter analyzer (2400S, Keithley Instruments) was employed for the characterization of electrochemical performance of the transistor. Patterned Au/Cr drain and source electrodes were deposited on glass slides by thermal evaporation (V22-300, KYKY Technology) using mask. The Cr layer (thickness: 5 nm) provides adhesion for Au layer (thickness: 70 nm). The morphologies of AuNPs/RGO nanocomposites were characterized using field emission scanning electron microscopy (FE-SEM, FEI, Tecnai, USA) and transmission electron microscopy (TEM, JEOL, 2100F, Japan). The crystalline structure of AuNPs/RGO nanocomposites was determined by X-ray diffraction (XRD, D8A25, BRUKER Technology Co., Ltd., Germany). The composition of AuNPs/RGO nanocomposites was investigated by X-ray photoelectron spectroscopy (XPS; PHOIBOS 150, SPECS). All experiments were carried out at room temperature.

3. Results and discussion

3.1. Morphology and composition of AuNPs/RGO nanocomposites

The surface morphologies of AuNPs/RGO nanocomposites prepared under optimal deposition conditions were characterized by FE-SEM and TEM. As can be seen from Fig. 2A and B, Au nanoparticles were uniformly distributed on GCE surface, and RGO was chiffon-like situated between Au nanoparticles to improve electron transport efficiency (He et al., 2019; Wang et al., 2018a,b,c). The average size of Au

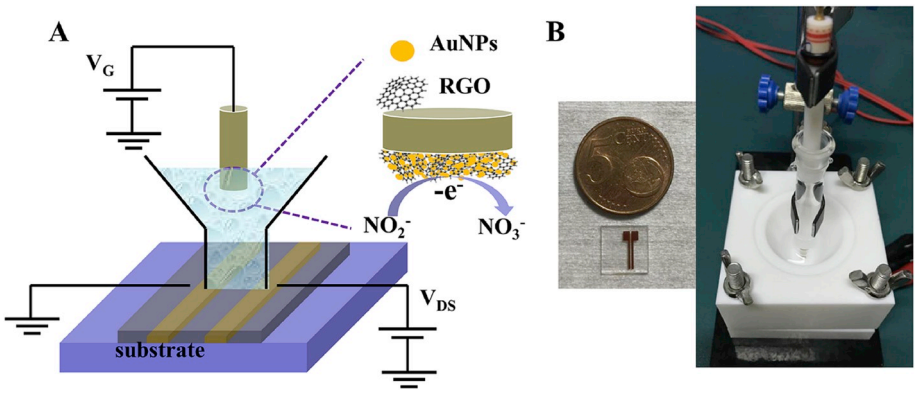

Fig. 1. (A) Schematic diagram of prepared GECT nitrite sensor. (B) Photographs for the glass substrate deposited with Au/Cr drain and source electrodes and the assembled actual device.

nanoparticles was estimated to be about 21 nm based on statistics of 50 particles in the inset TEM image of Fig. 2B. TEM indicated that Au nanoparticles were uniformly distributed in the flaky RGO films. AuNPs/RGO nanocomposites were formed and evenly covered on the GCE surface.

The crystalline structure of AuNPs/RGO nanocomposites were measured by XRD and the results are presented in Fig. S2A. The peaks of Au (111), (200), (220) and (311) planes were observed at 2θ of 38.2°, 44.4°, 64.6° and 77.5°, which is consistent with JCPDS card #65–8601, confirming the formation of AuNPs with typical face-centred cubic (fcc) structure. The broad peaks at 2θ of 25° and 45° in the inset of Fig. S2A were attributed to glassy carbon. To further characterize the composition of AuNPs/RGO nanocomposites, XPS was performed. The survey-scan spectrum (Fig. S2B) confirmed the presence of chemical elements of Au, C, and O in the nanocomposites by signals of Au4f/Au4d, C1s, and O1s, respectively. The main peaks of C1s related to C–C (284.5 eV) and C–O (286.4 eV) present in Fig. S2C (Stankovich et al., 2007) indicate that there were some oxygen-containing functional groups in RGO. These functional groups may play important roles in improving the attachment and the electrocatalytic activity of Au nanoparticles (Ismail et al., 2014; Shu et al., 2015). Additionally, two strong peaks appeared at 84.0 eV and 87.7 eV as seen in Fig. S2D, corresponding respectively to Au4f7/2 and Au4f5/2. The XPS analyses confirmed the successful preparation of AuNPs/RGO nanocomposites.

3.2. Electrochemical properties of AuNPs/RGO-modified GCE gated GECTs

3.2.1. Sensing principle and response towards nitrite

The bipolar behavior of graphene is clearly depicted in Fig. 3A. The Dirac point is greater than 0 V because graphene is p-type doped in water (Yavari et al., 2010; Zhang et al., 2014). Due to the zero-band gap structure of graphene, the electric field between the gate and channel would drive electrons from the valence band of graphene to conduction band to combine with holes. As voltage increased, the electrons gradually filled up the holes and then started to accumulate, resulting in first decreasing and then increasing carrier concentration in the graphene. Thus, the current in transfer curve decreased first and then increased, forming a V-shaped curve. The gate electrode modified with AuNPs/RGO nanocomposites was used as the working electrode, cyclic voltammetry was performed in 0.1 M phosphate buffer solution (pH = 7.4). Figure S3 shows the cyclic voltammograms from −0.2 to 1.5 V in phosphate buffer solution containing 1 mM nitrite with the scanning speed of 25 mV/s. It is seen that the addition of nitrite caused a significant increase of the oxidation peak around 0.8–0.9 V, indicating the occurrence of nitrite electrooxidation reaction on the surface of AuNPs/RGO nanocomposites. Thus, V_G value was set to 0.9 V for the following transistor tests.

The potential drop between the gate and source under V_G in PBS is depicted with blue line in Fig. 3B. The gate voltage applied on GECT devices would cross two interfaces, gate/electrolyte and electrolyte/channel, which can be described with $V_G = V_{G-E} + V_{E-C}$. The V_{E-C} was actually applied to the channel of the device. However, when nitrite is introduced in electrolyte solution, the potential difference at electrolyte/gate interface will be reduced by the electrooxidation of nitrite at the gate (Zhang et al., 2014) according to the Nernst Eq. (A):

$$V'_{G-E} = V_{G-E} - \frac{RT}{nF} ln C_{NO_2^-} \quad \text{(A)}$$

where n is the number of electrons lost during the electrochemical reaction, T is the absolute temperature, F is Faraday constant, and R is gas constant 8.3143 J/(K·mol).

Accordingly, the voltage applied to the electrolyte/channel interface increased, as shown in the red line of Fig. 3B. This, in turn, rose the

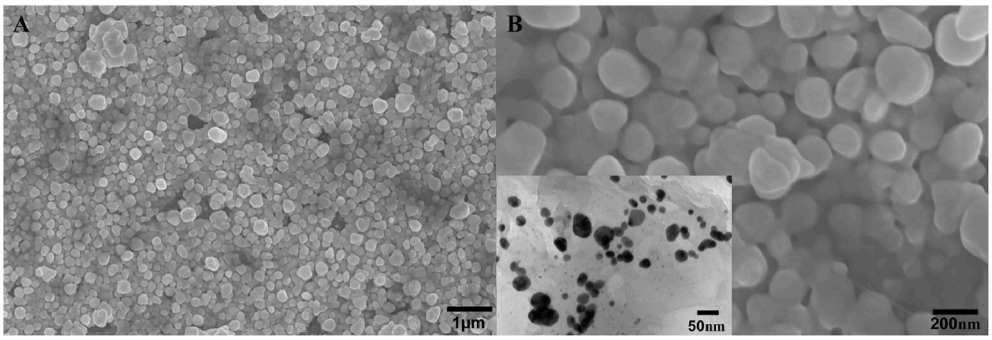

Fig. 2. FE-SEM images of AuNPs/RGO nanocomposites. (A)Zoom-out image and (B) Zoom-in image for the same area. Inset of B is TEM image of AuNPs/RGO nanocomposites after ultrasonic dispersion.

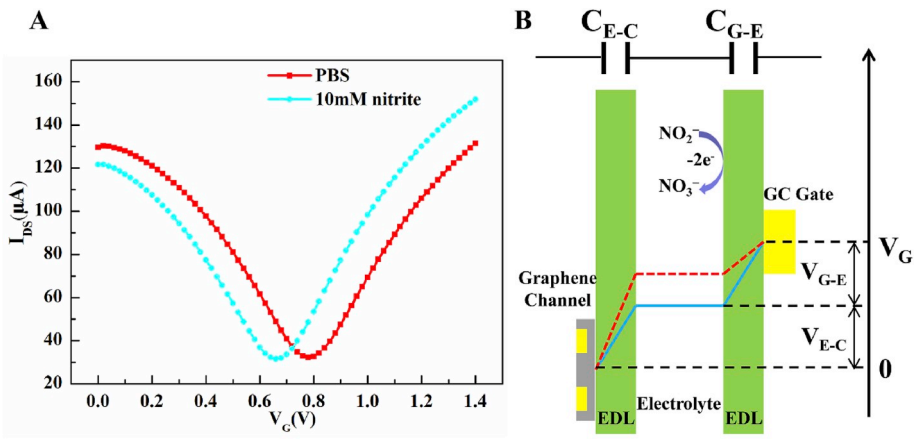

Fig. 3. (A) Transfer curve (I_{DS} vs. V_G, V_{DS} = 0.02 V) of a GECT measured in blank PBS (pH = 7.4) and PBS (pH = 7.4) with 10 M nitrite. (B) Schematic illustration of sensing principle of GECT towards nitrite.

effective gate voltage applied to GECT and shifted the transfer curve to lower voltages (Yan et al., 2014). Therefore, V_{E-C} became proportional to the logarithm of added nitrite concentration. Meanwhile, the channel current varied linearly with the gate voltage in narrow voltage range around 0.9 V (Fig. 3A) (Liao et al.,2015a; Bernards et al., 2008). So, the channel current was proportional to logarithm of the nitrite concentration following Eq. (B):

$$\Delta I_{DS} \propto ln C_{NO_2^-} \quad \text{(B)}$$

where ΔI_{DS} is the difference between channel currents before and after addition of the analyte.

3.2.2. Optimization of sensing performances

Different electrodeposition methods were employed to modify the gate electrode for best probing performances, including constant voltage deposition (AuNPs), stepwise deposition (AuNPs/RGO), cyclic voltammetry (AuNPs/RGO), and direct-current power deposition (AuNPs/RGO). The conditions of each modification method were optimized, as shown in Fig. S4. The sensing performances of GCE modified at the optimized conditions of each method were compared to blank GCE used as the gate of GECT for nitrite detection (Fig. 4). The results showed improvement in device performance after modification of the gate GCE with AuNPs or AuNPs/RGO nanocomposites when compared to bare GCE. Fig. 4F illustrates that sensing performances improved most obviously when AuNPs/RGO nanocomposites were deposited on the gate through cyclic voltammetry electrodeposition. Electrodeposition with 10 mM $HAuCl_4$, 0.5 mg/mL graphene oxide, and 0.1 M KCl aqueous solution using cyclic voltammetry from −1.2 V to 0.2 V for 10 circles at scan rate of 50 mV/s yielded the best sensing performance. The morphologies of AuNPs/RGO nanocomposites obtained by cyclic voltammetry with different scanning cycles were displayed in Fig. S5. It can be seen that as the number of scanning cycles increases, the size of the particles increases and the particles begin to stack. This could be attributed to the highest specific surface area and specific electrochemical active site of AuNPs.

3.2.3. Linearity and detection limit of optimized sensor

Fig. 5 shows the electrochemical characterization after modification of the GC gate with AuNPs/RGO nanocomposites at optimal conditions. Fig. 5A presents the response of the channel current (V_{DS} = 0.02 V and V_G = 0.9 V) to different nitrite concentrations. The detection limit of GECT reached 0.1 nM, and the detection range was linear from 0.1 nM to 7 μM and from 7 μM to 1 mM (Fig. 5B), better than those obtained by conventional electrochemical detection (Table 1). In "Guidelines for Drinking Water Quality, 2 nd Ed", World Health Organization stated that short-term exposure of nitrite should not exceed 3 mg/L (~65 μM). The national standard of China (GB/T8537-2008) stipulated that the hygienic standard for nitrite content in drinking natural mineral water is 0.005 mg/L (~100 nM). These prescribed nitrite contents are far beyond the detection lower-limit and fall satisfactorily into the detection range of our present GECT. Therefore, our GECT sensor devices hold brilliant prospects in detecting nitrite contents in highly demanding samples such as drinking mineral water and food. On the other hand, the current change between gate and source I_{GS} measured simultaneously was less than 100 nA (Fig. 5C), which was nearly 500 times lower than the channel current I_{DS}. This further illustrated that nitrite electrochemical reaction on the gate changed the effective gate voltage, leading to changes in the channel carrier concentration and thus the great change of channel current. This also confirmed that GECT can amplifier the electrochemical signal of nitrite, hence GECT performances were significantly superior to those of traditional electrochemical sensors.

3.2.4. Selectivity of optimized sensor

Selectivity of the sensor was evaluated by adding interfering species, including K^+, Ca^{2+}, Mg^{2+}, NH_4^+, Cl^-, NO^{3-}, SO_4^{2-}, PO_4^{3-}, CH_3COO^-, SO_3^{2-}, I^-, and glucose. As shown in Fig. 5D, the response to the addition of nitrite is remarkable, while the effect derived from the added anions and cations is negligible. The electroactive species such as SO_3^{2-}, I^-, and glucose also caused no apparent response, which might be due to different electrocatalytic reaction mechanisms involved on the surface of AuNPs/RGO nanocomposites. This indicated the detection of nitrite with the proposed structure can be performed without significant interference from the general interfering substances.

3.2.5. Stability and detection in standard samples

To further demonstrate the practicality of the present GECT sensor, it was repeatedly evaluated by detection of standard samples. The optimized GECT was tested 15 times towards detection of 1 mM nitrite and the responses are depicted in Fig. S6. The detected channel current change ΔI_{DS} varied between 93.5% and 107% of the initial value, showing good stability of the device. Known concentrations of nitrite were measured for three times and recovery values are listed in Table S1. Satisfactory recoveries in the range of 95–104.9% with maximum RSD error of 5.7% were revealed, further demonstrating the great potential of GECTs in direct analysis of standard samples. Both stability and recovery tests combined with the selectivity test indicate that the nonenzymatic GECTs proposed in this work hold great prospect for accurate nitrite detection of actual samples. To certify that our devices have a better practical outlook, different concentrations of nitrite samples were prepared by the water of East Lake (Wuhan, China) for recovery test. Through our tests, the lake water was not tested to contain nitrite. It could be seen from Table S2 that in the case of various interfering

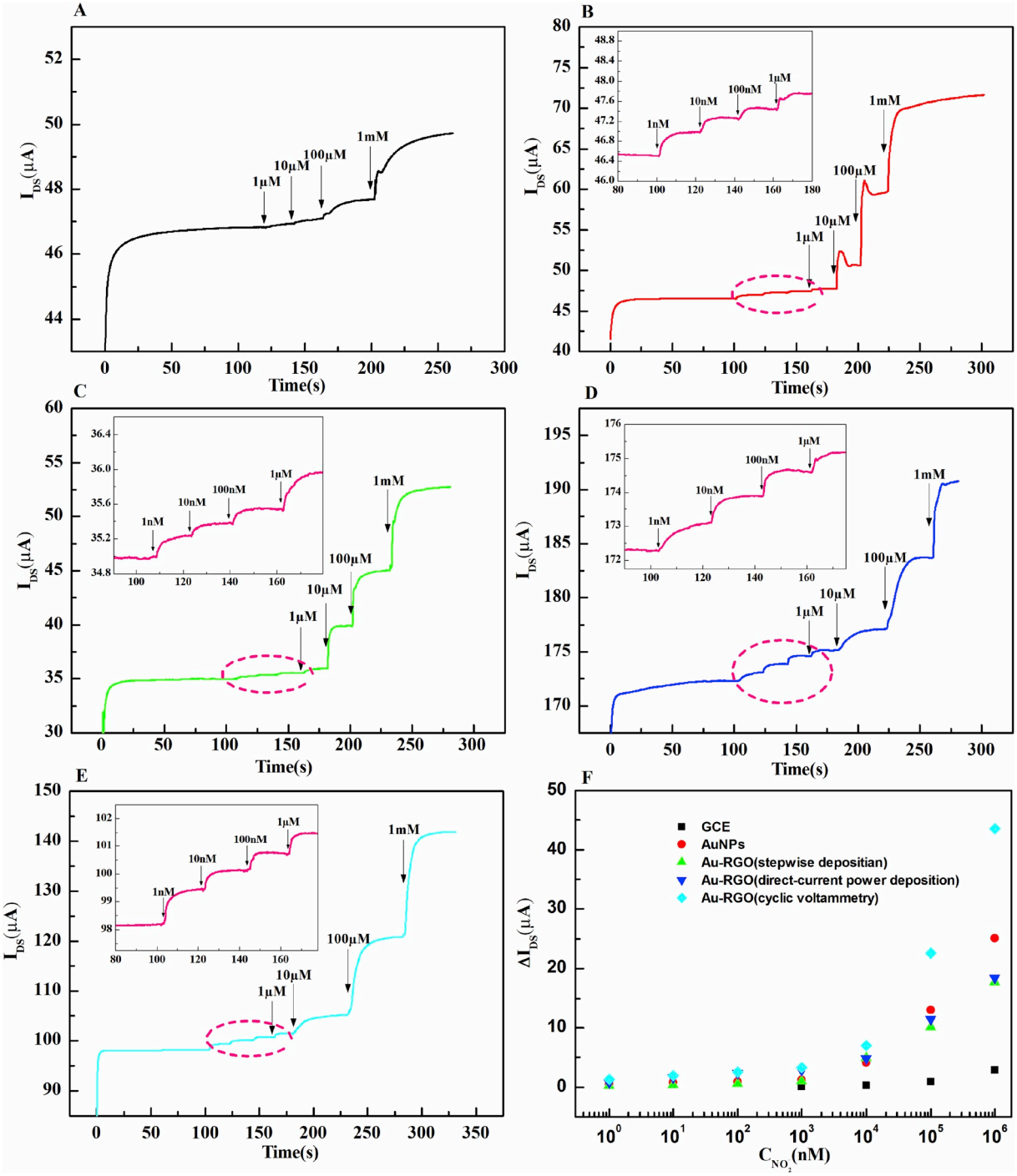

Fig. 4. Current-time curves ($V_G = 0.9$ V, $V_{DS} = 0.02$ V) of GECT with the gate electrode: unmodified (A), modified with AuNPs (B), and modified with AuNPs/RGO (C–E) nanocomposites. The measurements were performed in PBS solution (pH = 7.4) containing nitrite at different concentrations. The modification methods are: (B) constant voltage deposition method, (C) stepwise deposition, (D) direct-current power deposition, and (E) cyclic voltammetry. (F) Channel current responses ΔI_{DS} to various concentrations of nitrite for GECT with the gate electrode modified by different methods under optimal conditions.

substances in the water sample, the recovery rate of our test was basically kept within 87% ~124%. 3 nM nitrite in the lake water sample could be detected, indicating that our device is also competitive for trace detection of nitrite. This showed that our devices were capable of solving practical problems.

4. Conclusions

Highly sensitive nitrite sensors based on AuNPs/RGO nanocomposites modified graphene electrochemical transistors were designed and fabricated for the first time, in which AuNPs/RGO nanocomposites were electro-deposited on GCE as the gate electrode and graphene acted as the channel material of the devices. The modification effect of AuNPs/RGO nanocomposites on the GCE toward nitrite detection was systematically investigated by applying various modification methods and conditions, to optimize the novel composite gate electrode of the GECTs devices. Combining the current amplification principle of transistor, excellent electrocatalytic properties of AuNPs/

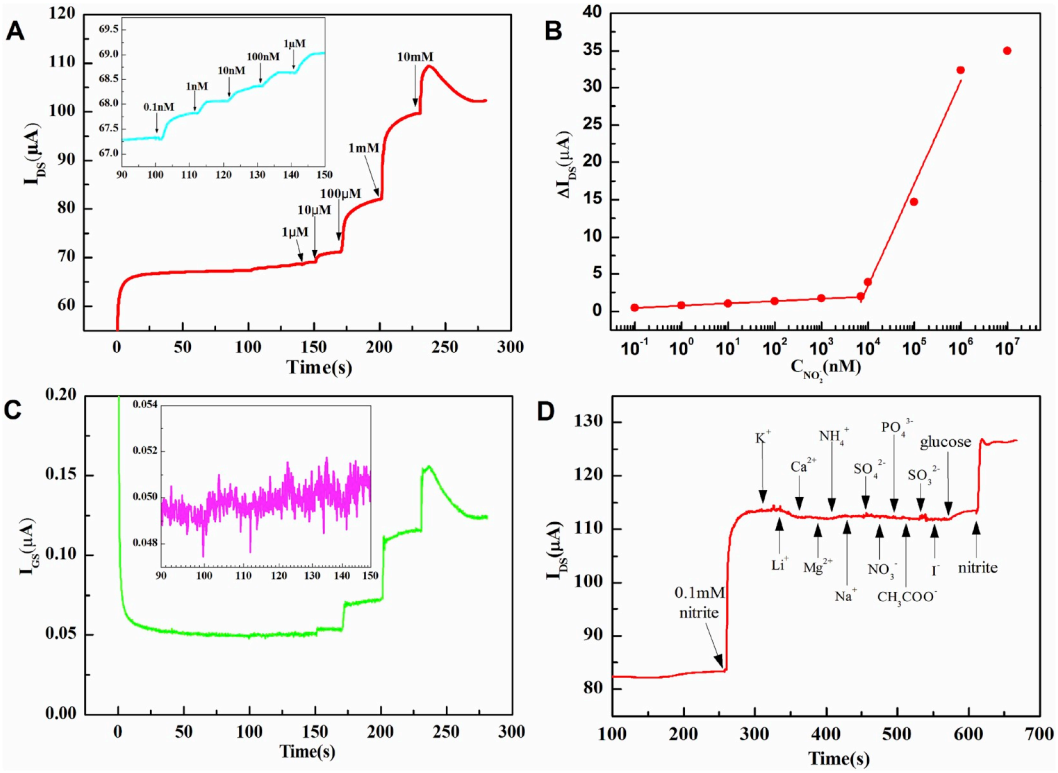

Fig. 5. (A) Channel current responses of GECT with AuNPs/RGO nanocomposites at gate to various additions of nitrite in PBS solution. Inset: magnification diagram of the low concentration part. (B) Fitting curve of changes of channel current (ΔI_{DS}) versus nitrite concentration. (C) Current responses between gate and source to additions of nitrite in PBS solution. Inset: magnification diagram of the low concentration part. (D) Anti-interference test with addition of 0.1 mM K^+, Li^+, Ca^{2+}, Mg^{2+}, NH_4^+, Cl^-, NO^{3-}, SO_4^{2-}, PO_4^{3-}, CH_3COO^-, SO_3^{2-}, I^-, and glucose against 0.1 mM nitrite.

Table 1
Comparison of properties between the GECT sensor prepared in this work and those prepared by traditional electrochemical methods.

Electrode	modification method	Linear range (μM)	Detection limit (μM)	Ref.
spectrophotometry	–	0.14–5.80	0.036	Zhao et al., (2015)
chromatography	–	0.029–0.43	0.0067	Zhang et al., (2018a)
spectrofluorimetry	–	0.0014–1.16	0.0005	Daneshvar Tarigh and Shemirani, (2014)
Fe_2O_3/RGO	Drop-cast	0.05–780	0.015	Radhakrishnan et al., (2014)
Fe_2O_3 NPs/ZnO NRs	Direct growth	1–1250	0.015	Ahmad et al., (2017)
Fe_3O_4/RGO	Drop-cast	0.5–58 0.5–9500	0.03	Bharath et al., (2015)
AuNPs/MWCPE	Direct growth	0.05–250	0.01	Afkhami et al., (2014)
Au/f-GE	Direct growth	0.125–20375.98	0.01	Zou et al., (2017)
AuNPs/ERGO	Direct growth	1–6000	0.13	Jian et al., (2018)
AuNPs/PEDOT	Drop-cast	0.2–1400	0.06	Lin et al., (2016)
Au-PtNPs	Drop-cast	0.5–1621	0.19	Li et al., (2016)
AuPd/UiO-66-NH_2	Direct growth	0.05–5666 5666–15666	0.01	Yang et al., (2016)
Ag-RGO	Drop-cast	0.1–120	0.012	Ahmad et al., (2018)
Px-CuO NSs	Drop-cast	0.1–1.8	0.012	Alsalme et al., (2018)
CNTs-TiN	Direct growth	1–2000	0.0014	Haldorai et al., (2016)
NPG films	Direct growth	1–110 110–200	0.01	Kumar et al., (2018)
NiHCF/PDAP	Direct growth	0.1–130	0.0151	Wang et al., (2018c)
$PMo_{11}V$/PDDA-rGO	Direct growth	0.125–1160	0.0028	Zhang et al., (2017)
PEI/PMo_9V_3/PEDOT/AuNPs	Direct growth	0.0025–1430	0.001	Zuo et al., (2016)
Au/RGO-GECT	Direct growth	0.0001–7 7–1000	0.0001	This work

RGO, and high carriers mobility and special surface of graphene, the as-prepared GECTs exhibited excellent performances towards the detection of nitrite with low detection limit (0.1 nM), broad linear range (0.1 nM −7 μM and 7–1000 μM), and good stability. The repeatability and detection of real samples illustrated the superior reliability of the sensors. All these indicated that GECTs based on AuNPs/RGO have great potential in developing novel high-performance nitrite sensors.

Declaration of competing interest

The authors declare that they have no known competing financial interests or personal relationships that could have appeared to influence the work reported in this paper.

CRediT authorship contribution statement

Yang Zhou: Methodology, Data curation, Formal analysis, Writing - original draft. **Mingyu Ma:** Methodology, Data curation, Formal analysis, Writing - review & editing. **Hanping He:** Formal analysis, Funding acquisition. **Zhiwei Cai:** Investigation, Visualization. **Nan Gao:** Methodology, Visualization. **Chaohui He:** Methodology. **Gang Chang:** Conceptualization, Funding acquisition, Project administration, Resources, Supervision. **Xianbao Wang:** Formal analysis, Resources. **Yunbin He:** Conceptualization, Funding acquisition, Project administration, Resources, Supervision.

Acknowledgements

This work was financially supported by the NSFC (Nos. 51572073, 21575035, 51672074, 11774082), the NSF of Hubei Province (Nos. 2015CFA119, 2016AAA031), Wuhan Application Foundation Frontier Project (No. 2018010401011287), and the Key Lab. of Tobacco Chemistry Foundation of Yunnan Province (No. 2016539200340109).

Appendix A. Supplementary data

Supplementary data to this article can be found online at https://doi.org/10.1016/j.bios.2019.111751.

References

Afkhami, A., Soltani-Felehgari, F., Madrakian, T., Ghaedi, H., 2014. Biosens. Bioelectron. 51, 379–385.
Ahmad, R., Ahn, M.-S., Hahn, Y.-B., 2017. Adv. Mater. Interfaces 4, 1700691.
Ahmad, R., Mahmoudi, T., Ahn, M.S., Yoo, J.Y., Hahn, Y.B., 2018. J. Colloid Interface Sci. 516, 67–75.
Alsalme, A., Arain, M., Nafady, A., Sirajuddin, 2018. Catalysts 8, 29.
Büldt, A., Karst, U., 1999. Anal. Chem. 71, 3003–3007.
Berggren, M., Richter-Dahlfors, A., 2007. Adv. Mater. 19, 3201–3213.
Bernards, D.A., Macaya, D.J., Nikolou, M., DeFranco, J.A., Takamatsu, S., Malliaras, G. G., 2008. J. Mater. Chem. A. 18, 116–120.
Bharath, G., Madhu, R., Chen, S.-M., Veeramani, V., Mangalaraj, D., Ponpandian, N., 2015. J. Mater. Chem. A. 3, 15529–15539.
Bru, M., Burguete, M.I., Galindo, F., Luis, S.V., Marín, M.J., Vigara, L., 2006. Tetrahedron Lett. 47, 1787–1791.
Daneshvar Tarigh, G., Shemirani, F., 2014. Talanta 128, 354–359.
Estrela, P., Paul, D., Song, Q., Stadler, L.K., Wang, L., Huq, E., Davis, J.J., Ko Ferrigno, P., Migliorato, P., 2010. Anal. Chem. 82, 3531–3536.
Faria, G.C., Duong, D.T., Salleo, A., 2017. Org. Electron. 45, 215–221.
Haldorai, Y., Hwang, S.K., Gopalan, A.I., Huh, Y.S., Han, Y.K., Voit, W., Sai-Anand, G., Lee, K.P., 2016. Biosens. Bioelectron. 79, 543–552.
Hao, Z., Zhu, Y., Wang, X., Rotti, P.G., DiMarco, C., Tyler, S.R., Zhao, X., Engelhardt, J.F., Hone, J., Lin, Q., 2017. ACS Appl. Mater. Interfaces 9, 27504–27511.
He, R.-X., Zhang, M., Tan, F., Leung, P.H.M., Zhao, X.-Z., Chan, H.L.W., Yang, M., Yan, F., 2012. J. Mater. Chem. 22, 22072.
Hempel, F., Law, J.K., Nguyen, T.C., Munief, W., Lu, X., Pachauri, V., Susloparova, A., Vu, X.T., Ingebrandt, S., 2017. Biosens. Bioelectron. 93, 132–138.
He, X., Luan, S.Z., Wang, L., Wang, R.Y., Du, P., Xu, Y.Y., Yang, H.J., Wang, Y.G., Huang, K., Lei, M., 2019. Mater. Lett. 244, 78–82.
Ismail, N.S., Le, Q.H., Yoshikawa, H., Saito, M., Tamiya, E., 2014. Electrochim. Acta 146, 98–105.
Jian, J.M., Fu, L., Ji, J., Lin, L., Guo, X., Ren, T.-L., 2018. Sens. Actuators B Chem. 262, 125–136.
Kodamatani, H., Yamazaki, S., Saito, K., Tomiyasu, T., Komatsu, Y., 2009. J. Chromatogr. A 1216, 3163–3167.
Kumar, A., Gonçalves, J.M., Sukeri, A., Araki, K., Bertotti, M., 2018. Sens. Actuators B Chem. 263, 237–247.
Li, Z., An, Z., Guo, Y., Zhang, K., Chen, X., Zhang, D., Xue, Z., Zhou, X., Lu, X., 2016. Talanta 161, 713–720.
Liao, J., Lin, S., Yang, Y., Liu, K., Du, W., 2015. Sens. Actuators B Chem. 208, 457–463.
Liao, C., Mak, C., Zhang, M., Chan, H.L., Yan, F., 2015. Adv. Mater. 27, 676–681.
Liao, C., Yan, F., 2013. Polym. Rev. 53, 352–406. Philadelphia, PA, U. S.
Liao, C., Zhang, M., Niu, L., Zheng, Z., Yan, F., 2013. J. Mater. Chem. B 1, 3820.
Lin, P., Chai, F., Zhang, R., Xu, G., Fan, X., Luo, X., 2016. Microchim. Acta 183, 1235–1241.
Lin, P., Yan, F., 2012. Adv. Mater. 24, 34–51.
Lin, P., Yan, F., Chan, H.L., 2010. ACS Appl. Mater. Interfaces 2, 1637–1641.
Lin, S., Bai, X., Wang, H., Wang, H., Song, J., Huang, K., Wang, C., Wang, N., Li, B., Lei, M., Wu, H., 2017. Adv. Mater. 29, e1703238.
Lin, S., Wang, H., Wu, F., Wang, Q., Bai, X., Zu, D., Song, J., Wang, D., Liu, Z., Li, Z., Tao, N., Huang, K., Lei, M., Li, B., Wu, H., 2019. npj Flex. Electron. 3, 6.
Mahajan, R.K., Kaur, R., Miyake, H., Tsukube, H., 2007. Anal. Chim. Acta 584, 89–94.
Mikuška, P., Večeřa, Z., 2003. Anal. Chim. Acta 495, 225–232.
Quhe, R., Liu, J., Wu, J., Yang, J., Wang, Y., Li, Q., Li, T., Guo, Y., Yang, J., Peng, H., Lei, M., Lu, J., 2019. Nanoscale 11, 532–540.
Radhakrishnan, S., Krishnamoorthy, K., Sekar, C., Wilson, J., Kim, S.J., 2014. Appl. Catal. B Environ. 148–149, 22–28.
Shu, H., Chang, G., Su, J., Cao, L., Huang, Q., Zhang, Y., Xia, T., He, Y., 2015. Sens. Actuators B Chem. 220, 331–339.
Stankovich, S., Dikin, D.A., Piner, R.D., Kohlhaas, K.A., Kleinhammes, A., Jia, Y., Wu, Y., Nguyen, S.T., Ruoff, R.S., 2007. Carbon 45, 1558–1565.
Tang, H., Lin, P., Chan, H.L., Yan, F., 2011. Biosens. Bioelectron. 26, 4559–4563.
Wang, X., Cui, Y., Li, T., Lei, M., Li, J., Wei, Z., 2018. Adv. Opt. Mater. 7, e1801274.
Wang, H., Liu, R., Li, Y., Lü, X., Wang, Q., Zhao, S., Yuan, K., Cui, Z., Li, X., Xin, S., Zhang, R., Lei, M., Lin, Z., 2018. Joule 2, 337–348.
Wang, X., Tan, W., Ji, H., Liu, F., Wu, D., Ma, J., Kong, Y., 2018. Sens. Actuators B Chem. 264, 240–248.
Wei, J., Guo, F., Wang, X., Xu, K., Lei, M., Liang, Y., Zhao, Y., Xu, D., 2018. Adv. Mater. 30, e1805153.
Wolfe, A.H., Patz, J.A., 2002. Ambio 31, 120–125.
Yan, F., Zhang, M., Li, J., 2014. Adv. Healthc. Mater. 3, 313–331.
Yang, J., Yang, L., Ye, H., Zhao, F., Zeng, B., 2016. Electrochim. Acta 219, 647–654.
Yavari, F., Kritzinger, C., Gaire, C., Song, L., Gulapalli, H., Borca-Tasciuc, T., Ajayan, P. M., Koratkar, N., 2010. Small 6, 2535–2538.
Zhang, L., Li, S., Zhang, Z., Tan, L., Pang, H., Ma, H., 2017. J. Electroanal. Chem. 807, 97–103.
Zhang, L., Wang, G., Wu, D., Xiong, C., Zheng, L., Ding, Y., Lu, H., Zhang, G., Qiu, L., 2018. Biosens. Bioelectron. 100, 235–241.
Zhang, M., Liao, C., Yao, Y., Liu, Z., Gong, F., Yan, F., 2014. Adv. Funct. Mater. 24, 978–985.
Zhang, S.X., Peng, R., Jiang, R., Chai, X.S., Barnes, D.G., 2018. J. Chromatogr., A 1538, 104–107.
Zhao, J., Lu, Y., Fan, C., Wang, J., Yang, Y., 2015. Spectrochim. Acta A Mol. Biomol. Spectrosc. 136, 802–807.
Zou, C., Yang, B., Bin, D., Wang, J., Li, S., Yang, P., Wang, C., Shiraishi, Y., Du, Y., 2017. J. Colloid Interface Sci. 488, 135–141.
Zuo, J., Zhang, Z., Jiao, J., Pang, H., Zhang, D., Ma, H., 2016. Sens. Actuators B Chem. 236, 418–424.